Electronic Supplementary Material (ESI) for Dalton Transactions.
This journal is © The Royal Society of Chemistry 2017

Electronic Supplementary Information

Influence of Thiolate ligands on Luminescent Properties of Cycloplatinated(II) Complexes

Mahboubeh Jamshidi,[a] Mojgan Babaghasabha,[b] Hamid R. Shahsavari,[b]* and S. Masoud Nabavizadeh,[a]*

[a]*Department of Chemistry, College of Sciences, Shiraz University, Shiraz 71454, Iran.*

[b]*Department of Chemistry, Institute for Advanced Studies in Basic Sciences (IASBS), Yousef Sobouti Blvd., Zanjan 45137-66731, Iran.*

*Email: shahsavari@iasbs.ac.ir. (H.R.S.); nabavizadeh@shirazu.ac.ir. (S.M.N)

Contents:	Page
Figure S1. ^{1}H NMR spectrum of **1a** in dmso-d_6 at room temperature.	S3
Figure S2. ^{31}P{^{1}H} NMR spectrum of **1a** in dmso-d_6 at room temperature.	S3
Figure S3. ^{1}H NMR spectrum of **2a** in dmso-d_6 at room temperature.	S4
Figure S4. ^{31}P{^{1}H} NMR spectrum of **2a** in dmso-d_6 at room temperature.	S4
Figure S5. ^{1}H NMR spectrum of **3a** in dmso-d_6 at room temperature.	S5
Figure S6. ^{31}P{^{1}H} NMR spectrum of **3a** in dmso-d_6 at room temperature.	S5
Figure S7. ^{1}H NMR spectrum of **3b** in dmso-d_6 at room temperature.	S6
Figure S8. ^{31}P{^{1}H} NMR spectrum of **3b** in dmso-d_6 at room temperature.	S6
Table S1. Crystallographic and structure refinement data for **1a** and **2a**.	S7
Table S2. Selected Distances [A] and Angles [^{o}] for **1a**, **2a** and **1b**.	S8
Figure S9. Aromatic ring including the κ^1-S-SR moiety is approximately perpendicular to the metal plane. The dihedral angle between the metal plane and the aryl ring is 82.88˚ for **1a** and 63.24˚ for **2a**.	S8
Figure 10. Crystal packing of complexes (a) **1a** and (b) **2a** are displaying the intermolecular and intramolecular contacts. The supramolecular packing is formed by dimers supported by intermolecular π···π interactions involving two bzq ligands. Hydrogen atoms have been omitted for clarity.	S9
Table S3. Absorption data for **A**, **B**, **1-3** and some ligands in CH_2Cl_2 solutions and solid state at ambient temperature.	S10
Figure S11. UV-vis spectra of **1a** and **1b** in CH_2Cl_2 at 298 K.	S11
Figure S12. Absorption spectra of (a) **A**, **1a**, **2a** and **3a**; (b) **B**, **1b**, **2b** and **3b** in solid state at 298 K.	S12
Table S4. Selected low-lying singlet and triplet excited states computed by TD-DFT with the orbitals involved and vertical excitation energies (nm) for **1-3**.	S13
Table S5. Composition (%) of frontier MOs in the ground state (S_0) for complexes **1-3** in gas phase.	S14
Figure S13. DFT optimized S_0 (left) and T_1 (right) geometries of complex **3b** with corresponding contribution of different fragments in frontier molecular orbitals obtained in S_0 and T_1 states.	S15
Figure S14. Emission spectra of (a) **1a** and (b) **1b** in solid, PMMA and PS films at 298 K.	S16

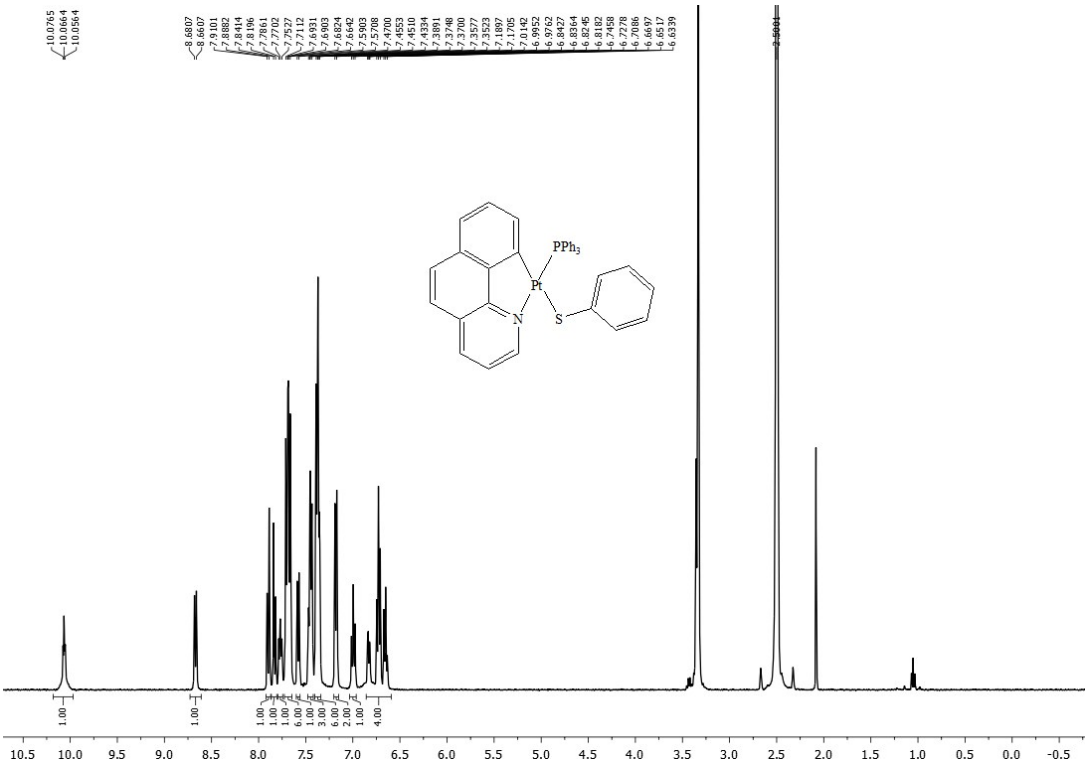

Figure S1. ^{1}H NMR spectrum of **1a** in dmso-d_6 at room temperature.

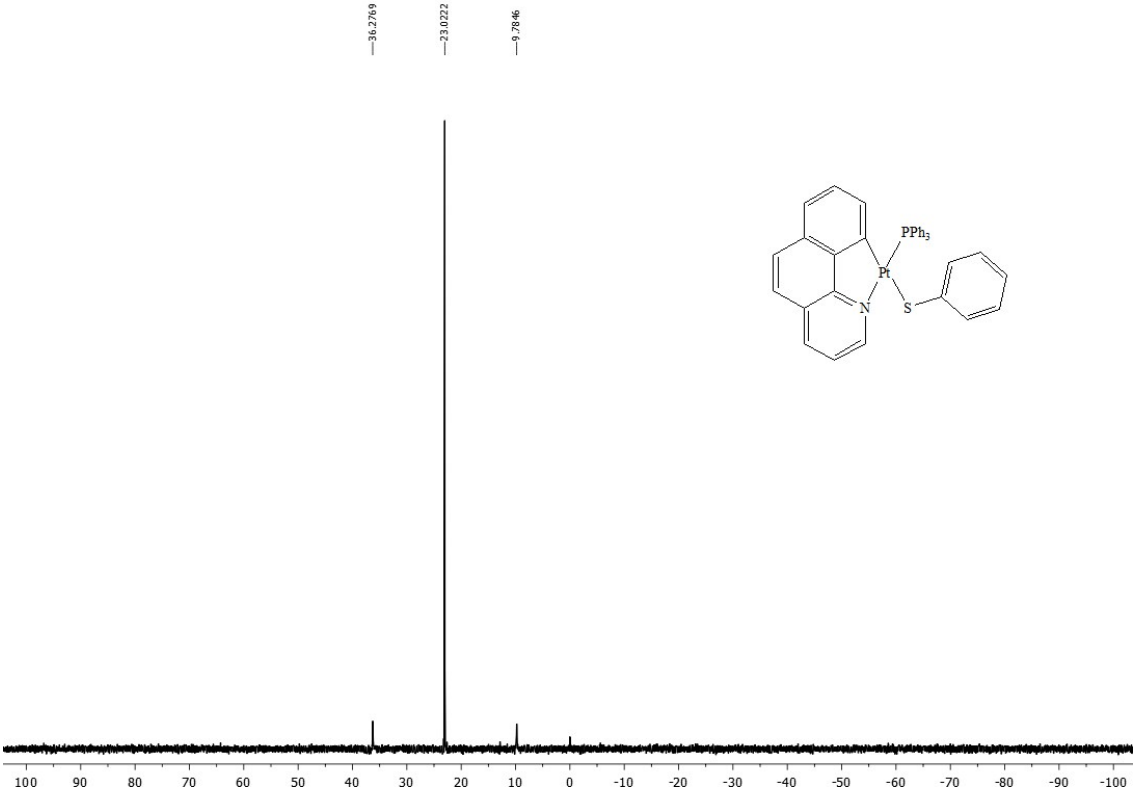

Figure S2. ^{31}P{^{1}H} NMR spectrum of **1a** in dmso-d_6 at room temperature.

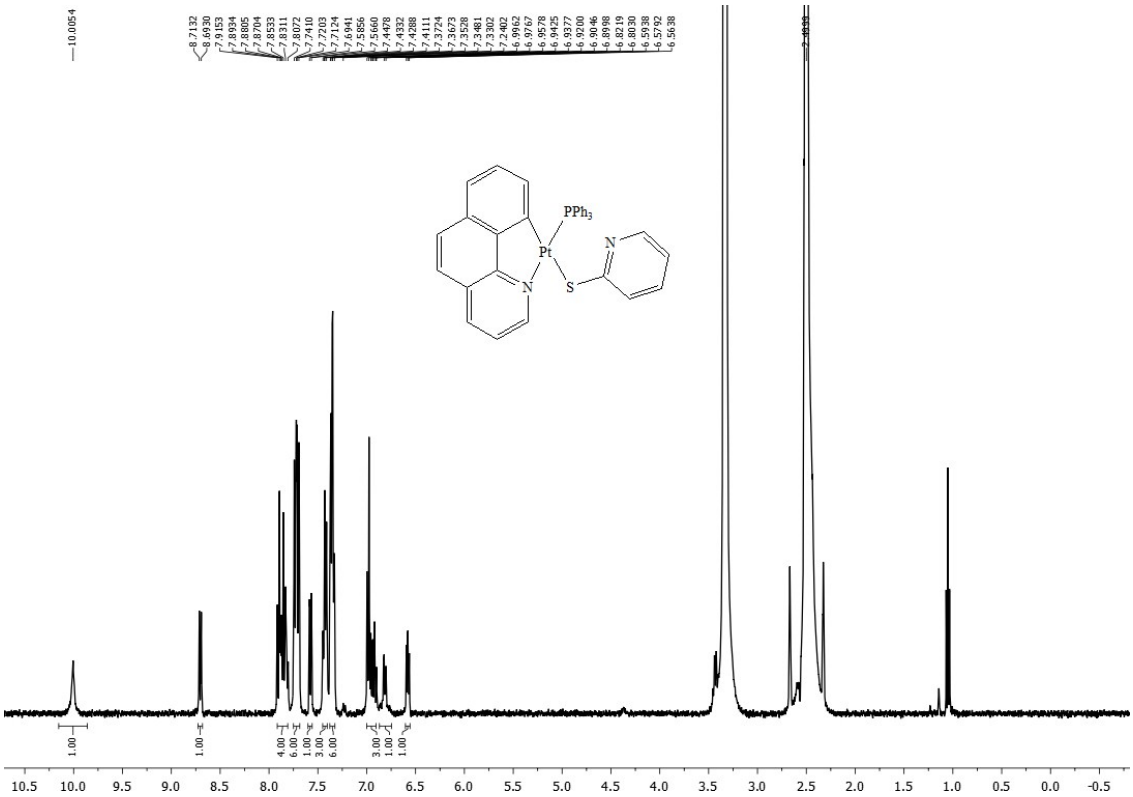

Figure S3. ^{1}H NMR spectrum of **2a** in dmso-d_6 at room temperature.

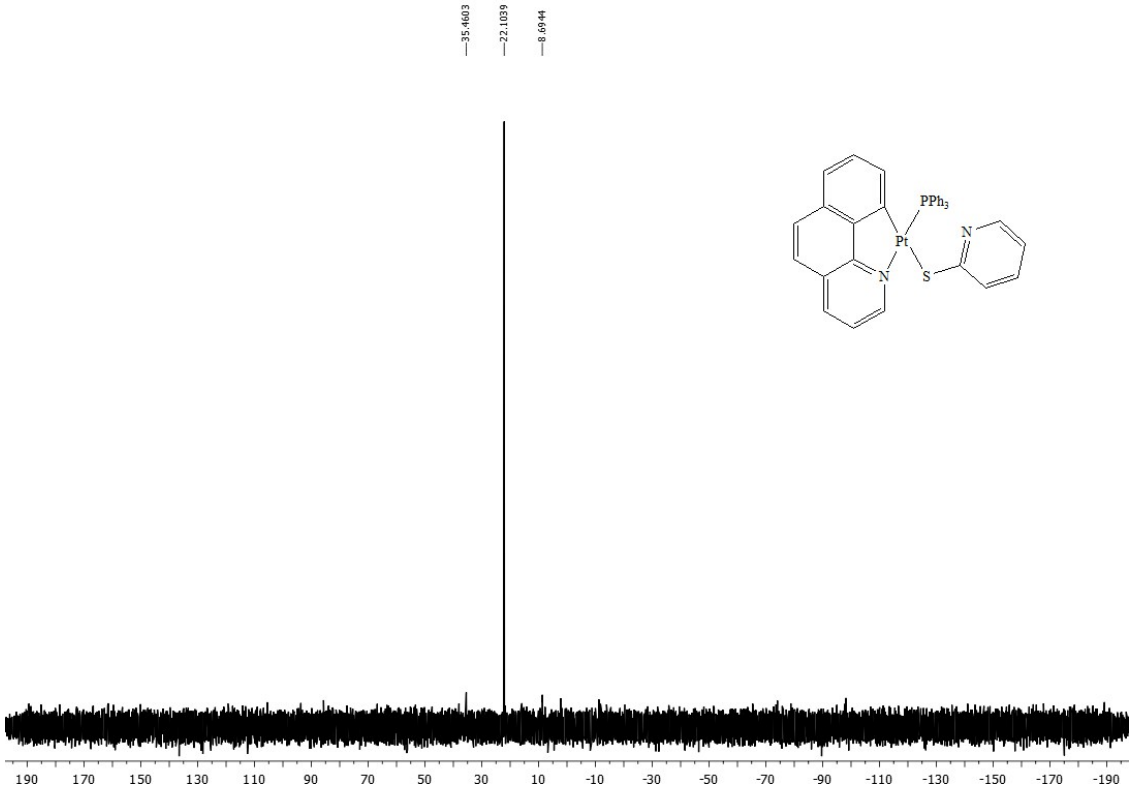

Figure S4. ^{31}P{^{1}H} NMR spectrum of **2a** in dmso-d_6 at room temperature.

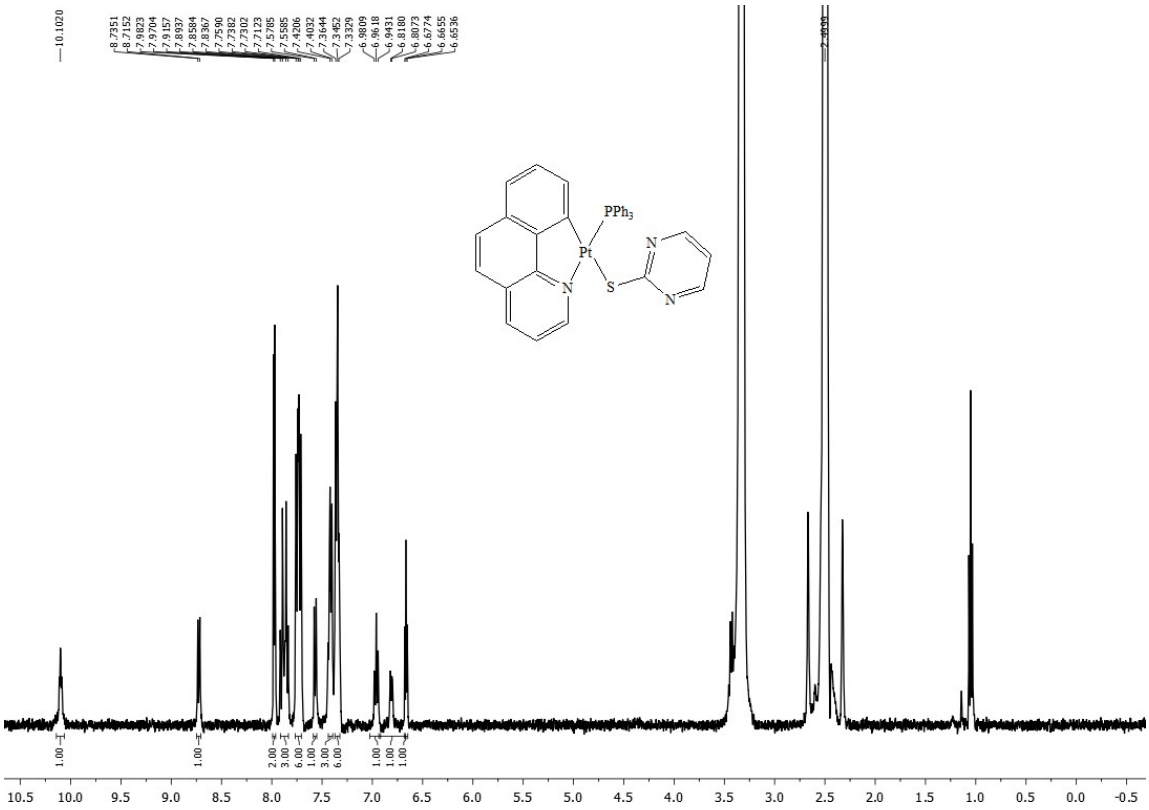

Figure S5. ^{1}H NMR spectrum of **3a** in dmso-d_6 at room temperature.

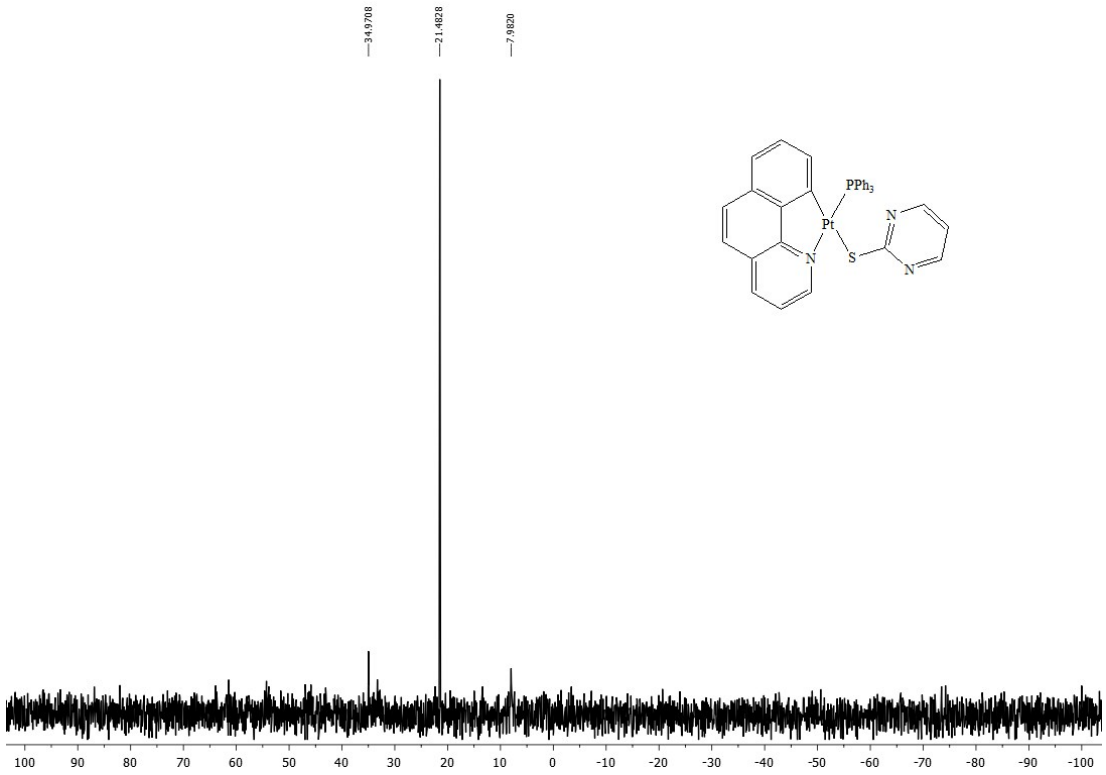

Figure S6. ^{31}P{^{1}H} NMR spectrum of **3a** in dmso-d_6 at room temperature.

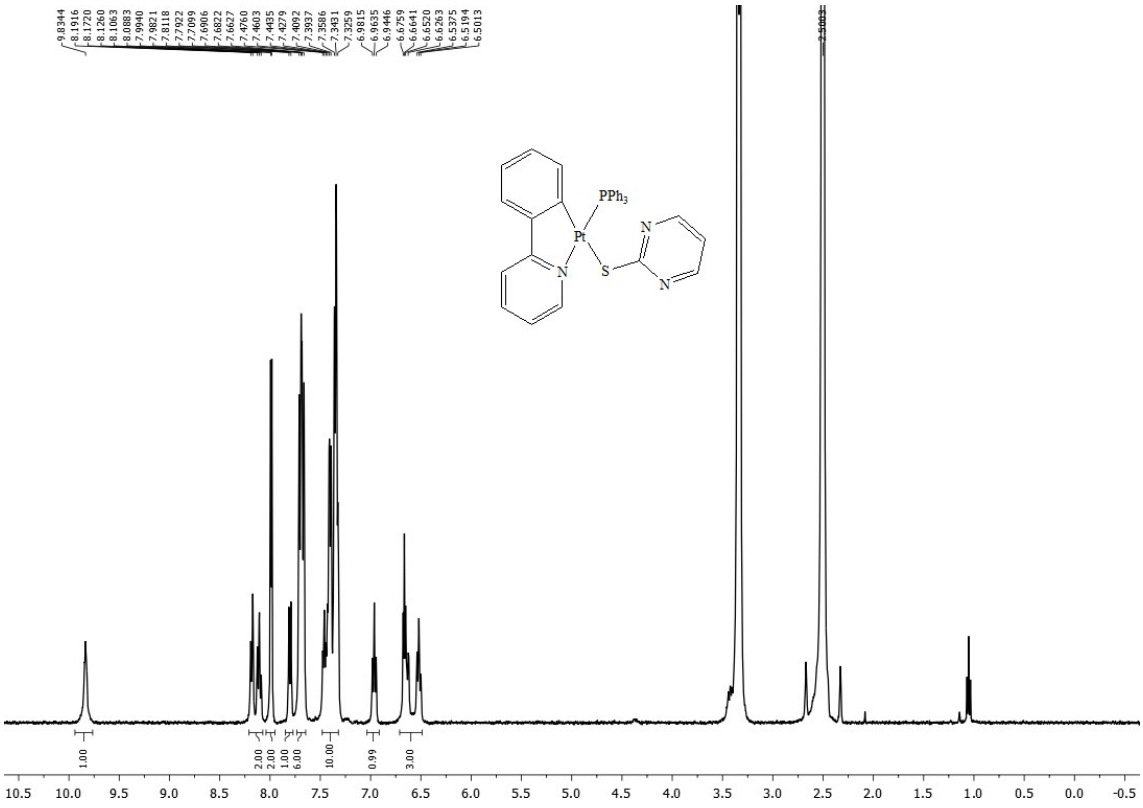

Figure S7. ^{1}H NMR spectrum of **3b** in dmso-d_6 at room temperature.

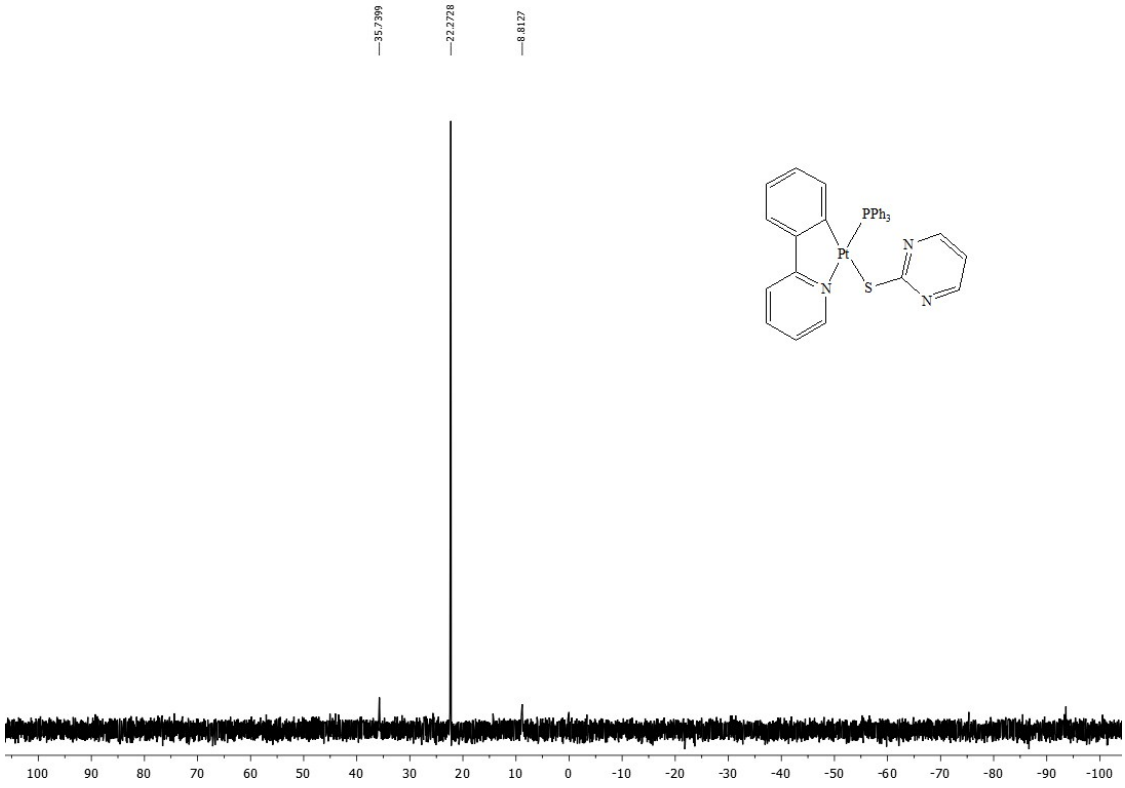

Figure S8. ^{31}P{^{1}H} NMR spectrum of **3b** in dmso-d_6 at room temperature.

Table S1. Crystallographic and structure refinement data for **1a** and **2a**.

Compound	**1a**	**2a**
Formula	$C_{38}H_{30}Cl_2NPPtS$	$C_{36}H_{27}N_2PPtS$
$D_{calc.}$/ g cm^{-3}	1.711	1.713
m/mm^{-1}	10.973	10.491
Formula Weight	829.65	745.71
Color	yellow	clear yellow
Shape	prism	prism
T/K	294.60(10)	123.01(10)
Crystal System	triclinic	monoclinic
Space Group	P-1	$P2_1/n$
a/Å	10.0395(2)	19.6231(3)
b/Å	10.9690(2)	8.23150(10)
c/Å	15.0116(3)	20.0833(3)
a/°	85.1370(10)	90
b/°	85.669(2)	116.938(2)
g/°	78.299(2)	90
V/Å^3	1610.06(6)	2892.02(8)
Z	2	4
Z'	1	1
Wavelength/Å	1.54184	1.54184
Radiation type	CuK_a	CuK_a
Q_{min}/°	4.126	4.259
Q_{max}/°	73.664	73.689
Measured Refl.	34429	60590
Independent Refl.	6395	5804
Reflections Used	6270	5460
R_{int}	0.0503	0.0426
Parameters	397	370
Restraints	0	0
Largest Peak	0.602	1.242
Deepest Hole	-0.980	-0.899
GooF	1.057	1.063
wR_2 (all data)	0.0452	0.0442
wR_2	0.0449	0.0433
R_1 (all data)	0.0192	0.0203
R_1	0.0187	0.0183
CCDC No.	1547213	1547214

Table S2. Selected Distances [A] and Angles [°] for **1a**, **2a** and **1b**.

	1a	**2a**	**1b**
Pt-S(1)	2.3689(6)	2.3651(6)	2.361(3)
Pt-N(1)	2.0951(19)	2.1073(19)	2.073(9)
Pt-C(1)	2.043(2)	2.048(2)	2.065(12)
Pt-P(1)	2.2285(6)	2.2228(6)	2.244(3)
C(1)-Pt-N(1)	80.84(9)	80.76(9)	81.9(4)
N(1)-Pt-S(1)	91.88(6)	90.63(6)	90.2(3)
S(1)-Pt-P(1)	93.00(2)	93.85(2)	90.95(11)
P(1)-Pt-C(1)	94.34(7)	94.75(7)	97.2(3)
Pt-S(1)-C(14)	107.58(8)	109.51(8)	107.1(5)

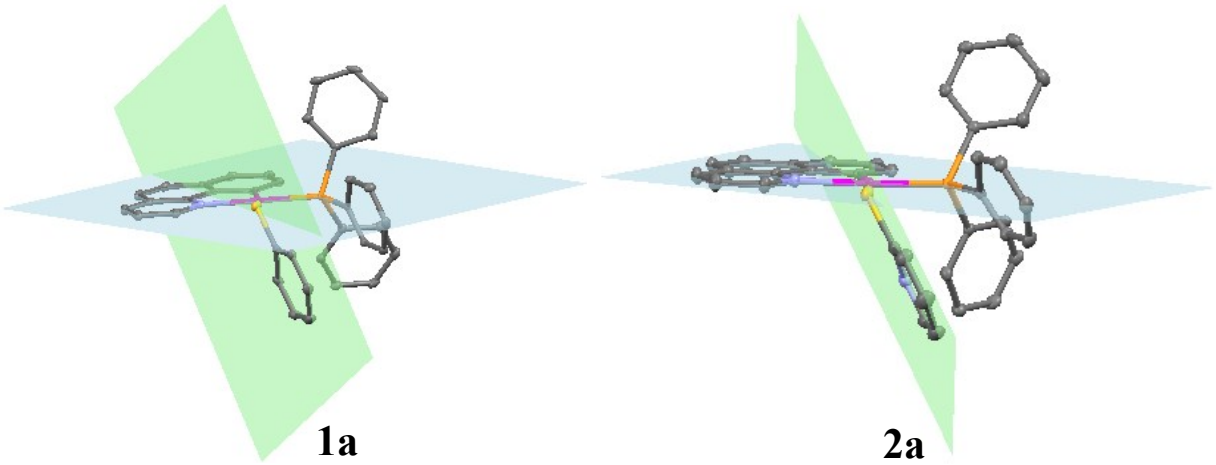

Figure S9. Aromatic ring including the κ^1-S-SR moiety is approximately perpendicular to the metal plane. The dihedral angle between the metal plane and the aryl ring is 82.88˚ for **1a** and 63.24˚ for **2a**.

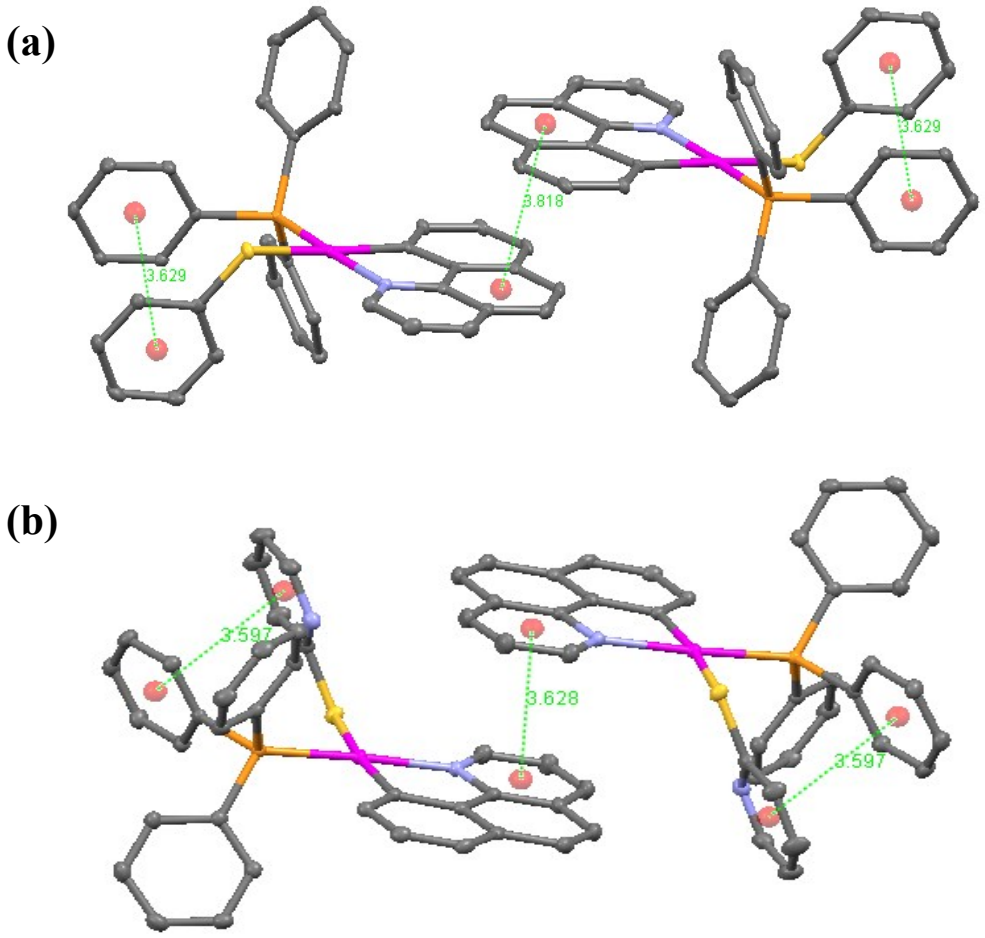

Figure 10. Crystal packing of complexes (a) **1a** and (b) **2a** showing the intermolecular and intramolecular contacts. The supramolecular packing is formed by dimers supported by intermolecular π···π interactions involving two bzq ligands. Hydrogen atoms are omitted for clarity.

Table S3. Absorption data for **A**, **B**, **1-3** and some ligands in CH_2Cl_2 solutions and solid state at ambient temperature.

Compound	**media**	**λ_{abs}/nm (ε / 10^{-4} M^{-1} cm^{-1})**
Free bzqH	CH_2Cl_2 (10^{-3} M)	296(4.49), 330(4.31), 345(4.37)
Free Na^+Spy^-	CH_2Cl_2 (2×10^{-5} M)	282(4.21), 359(3.80)
Free SpyH	CH_2Cl_2 (2×10^{-5} M)	292(4.16), 375(3.73)
A	CH_2Cl_2 (5×10^{-5}M)	235(4.59), 261(4.52), 305(4.16), 328(3.78), 340(3.53), 394(3.25),416(3.53)
	Solid	229, 265, 315, 401, 418, 468, 593
B	CH_2Cl_2 (5×10^{-5}M)	232(4.46), 287(4.26), 315(3.71), 327(3.55), 328(3.28)
	Solid	230, 268, 289, 320, 382, 445, 478
1a	CH_2Cl_2 (5×10^{-5}M)	244(4.70), 276(4.34), 287(4.35), 346(3.74), 374(3.59), 399(3.39), 450(2.89)
	Solid	240, 268, 310, 410, 474, 621
1b	CH_2Cl_2 (5×10^{-5}M)	231(4.83), 277(4.45), 326(3.97), 364(3.53), 438(3.11)
	Solid	209, 234, 270, 325, 370, 463, 502
2a	CH_2Cl_2 (5×10^{-5}M)	241(4.69), 287(4.34), 348(3.86), 397(3.42), 432(3.15)
	Solid	234, 298, 370, 448, 535, 635
2b	CH_2Cl_2 (5×10^{-5}M)	284(4.00), 326(3.94), 386(3.40), 417(3.18)
	Solid	205, 232, 271, 357, 451, 532
3a	CH_2Cl_2 (5×10^{-5}M)	234(4.79), 288(4.37), 347(3.79), 413(3.33)
	Solid	232, 295, 345, 382, 420, 418, 633
3b	CH_2Cl_2 (5×10^{-5}M)	237(4.46), 274(4.52), 329(4.04), 392(3.34)
	Solid	229, 273, 330, 375, 443

[a]Data at high concentration (10^{-3} M) are similar to those at low concentration.

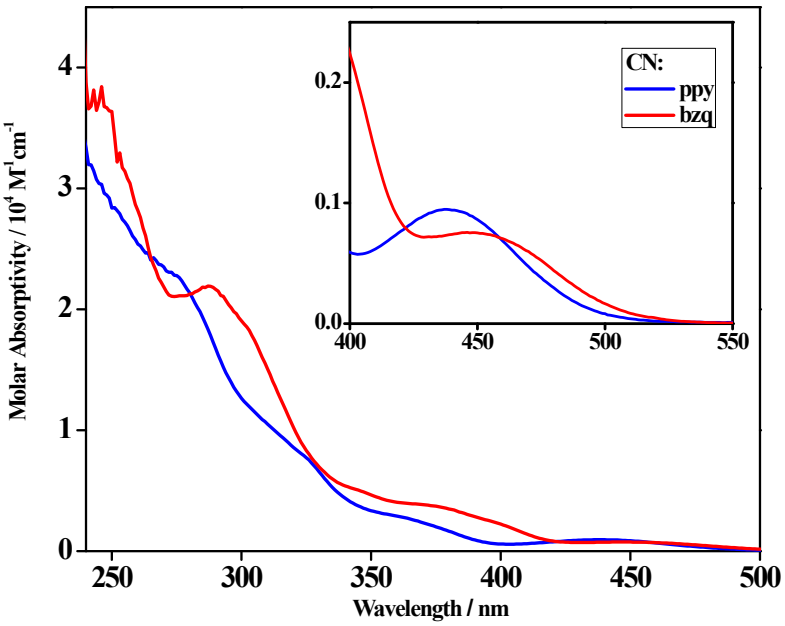

Figure S11. UV-vis spectra of **1a** and **1b** in CH_2Cl_2 at 298 K (the insets show the expansion of the region of the low-energy bands).

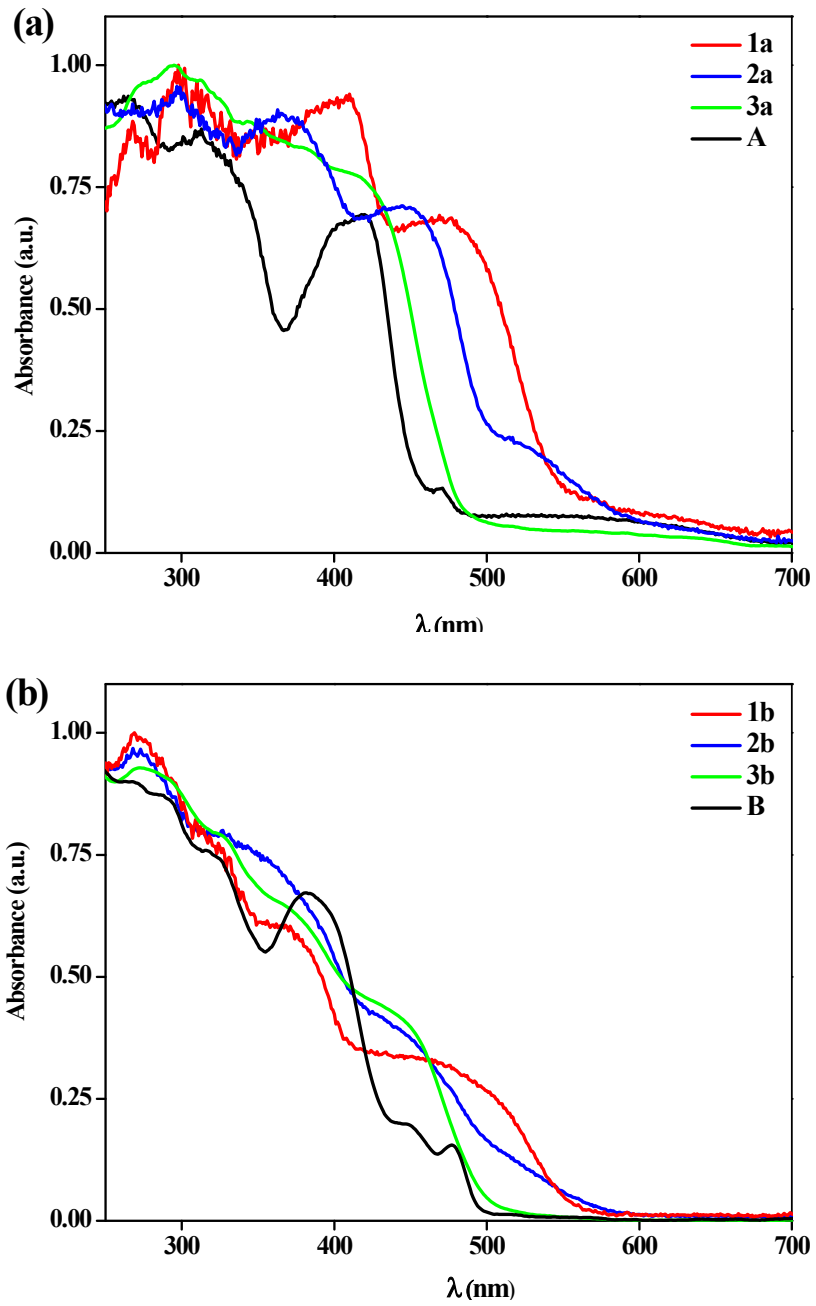

Figure S12. Absorption spectra of (a) **A**, **1a**, **2a** and **3a**; (b) **B**, **1b**, **2b** and **3b** in solid state at 298 K.

Table S4. Selected low-lying singlet and triplet excited states computed by TD-DFT with the orbitals involved and vertical excitation energies (nm) for **1-3**.

	State	λ_{exc} (calc.)/nm	*f*	Main Transition (Percentage Contribution)
1a	T_1	621		HOMO→LUMO (98)
	S_1	572	0.003	HOMO→LUMO (98)
	S_2	441	0.003	HOMO→LUMO+1 (95)
	S_3	429	0.013	HOMO→LUMO+3 (77)
2a	T_1	540		HOMO→LUMO (98)
	S_1	514	0.002	HOMO→LUMO (98)
	S_2	405	0.003	HOMO→LUMO+1 (95)
	S_3	394	0.004	HOMO→LUMO+3 (84)
	S_4	388	0.043	HOMO-1→LUMO (92)
3a	T_1	480		HOMO→LUMO (90)
	S_1	474	0.002	HOMO→LUMO (98)
	S_2	378	0.038	HOMO-1→LUMO (92)
	S_3	379	0.004	HOMO→LUMO (90)
1b	T_1	607		HOMO→LUMO (98)
	S_1	522	0.005	HOMO→LUMO (98)
	S_2	433	0.007	HOMO→LUMO+3 (70)
	S_3	419	0.002	HOMO→LUMO+2 (52) HOMO→LUMO+1 (26)
2b	T_1			HOMO→LUMO (98)
	S_1	523	0.003	HOMO→LUMO (98)
	S_2	414	0.004	HOMO→LUMO+3 (72)
	S_3	401	0.002	HOMO→LUMO+2 (44) HOMO→LUMO+1 (32)
3b	T_1			HOMO→LUMO (77)
	S_1	454	0.003	HOMO→LUMO (98)
	S_2	372	0.000	HOMO→LUMO+3 (70)
	S_3	369	0.046	HOMO-1→LUMO (82)

Table S5. Composition (%) of frontier MOs in the ground state (S_0) for complexes **1**-**3** in gas phase.

	E (eV)	Pt	bzq	SR	PPh_3
1a					
L+3	-0.781	26	11	6	57
L+2	-0.885	9	5	0	87
L+1	-1.081	3	88	3	5
LUMO	-1.673	3	93	1	4
HOMO	-4.452	8	8	81	3
H-1	-5.465	23	43	32	2
H-2	-5.689	13	48	37	3
H-3	-6.022	55	4	36	5
2a					
L+3	-0.684	28	12	5	55
L+2	-0.797	6	4	0	90
L+1	-1.013	3	90	3	4
LUMO	-1.611	3	93	1	3
HOMO	-4.630	8	6	83	3
H-1	-5.462	31	61	7	1
H-2	-5.772	63	2	30	6
H-3	-5.895	10	42	45	3
3a					
L+3	-0.729	27	11	6	56
L+2	-0.842	7	4	1	88
L+1	-1.041	3	90	3	4
LUMO	-1.640	3	93	1	3
HOMO	-4.878	10	6	81	3
H-1	-5.495	31	61	7	1
H-2	-5.711	22	14	61	4
H-3	-5.927	50	28	17	4

	E (eV)	Pt	ppy	SR	PPh_3
1b					
L+3	-0.770	27	13	5	55
L+2	-0.848	2	71	2	26
L+1	-0.901	8	15	0	77
LUMO	-1.552	5	87	2	6
HOMO	-4.418	7	7	82	3
H-1	-5.563	23	33	42	2
H-2	-5.773	25	49	25	2
H-3	-6.025	37	2	57	3
2b					
L+3	-0.797	27	14	5	53
L+2	-0.890	2	68	1	29
L+1	-0.938	7	15	1	78
LUMO	-1.593	5	87	2	6
HOMO	-4.592	7	6	83	3
H-1	-5.676	35	41	23	1
H-2	-5.786	12	34	52	2
H-3	-6.039	2	13	84	1
3b					
L+3	-0.710	27	10	6	57
L+2	-0.815	2	36	1	61
L+1	-0.852	7	18	0	75
LUMO	-1.505	5	68	2	26
HOMO	-4.871	9	5	81	4
H-1	-5.603	43	34	9	14
H-2	-5.698	21	11	63	5
H-3	-5.904	52	23	16	9

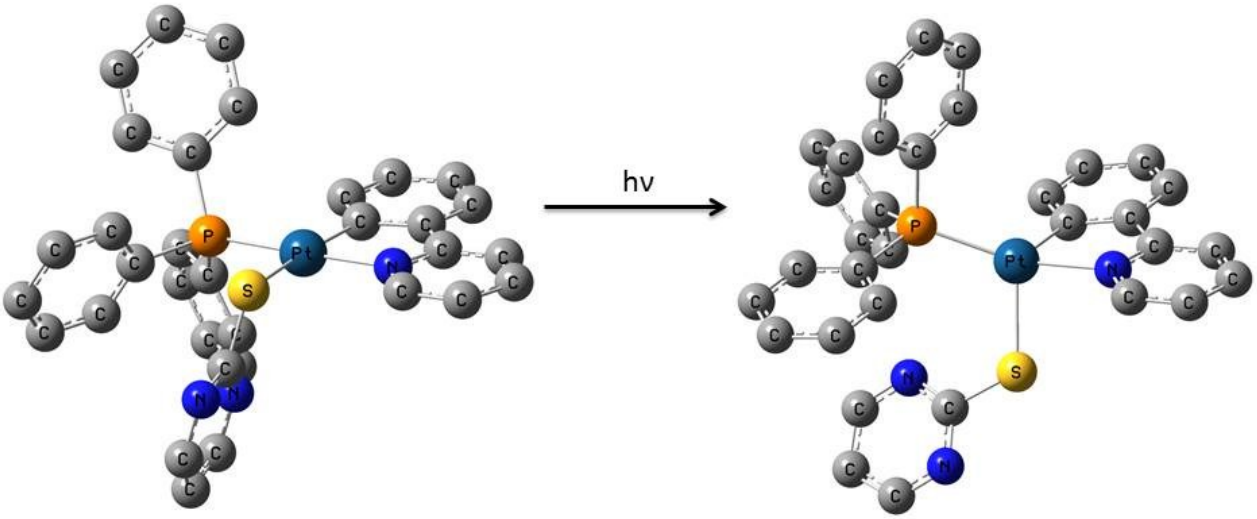

S_0	Pt	SpyN	ppy	PPh_3
LUMO	5	2	68	26
HOMO	9	81	5	4

T_1	Pt	SpyN	ppy	PPh_3
HSOMO	34	9	29	27
LSOMO	39	39	12	9

Figure S13. DFT optimized S_0 (left) and T_1 (right) geometries of complex **3b** with corresponding contribution of different fragments in frontier molecular orbitals obtained in S_0 and T_1 states.

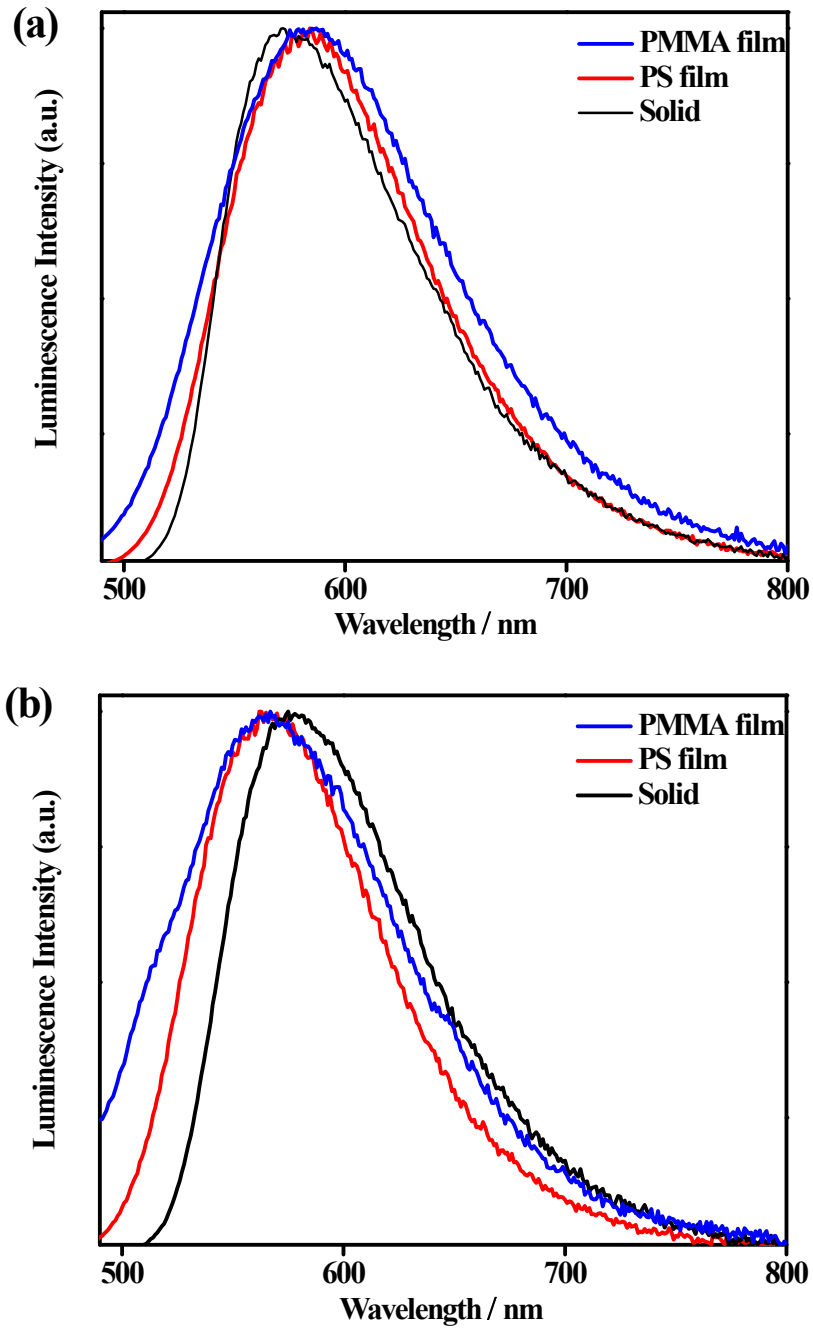

Figure S14. Emission spectra of (a) **1a** and (b) **1b** in solid, PMMA and PS films at 298 K.